AGU PUBLICATIONS

Geophysical Research Letters

RESEARCH LETTER
10.1002/2014GL062518

Key Points:
- Extension of the Matsuno-Gill model to the sphere with mean subtropical jets
- Transition from a Rossby wave train to a subtropical quadrupole is demonstrated
- Implications for the upper level structure of the MJO are discussed

Supporting Information:
- Readme
- Figure S1
- Figure S2
- Figure S3
- Table S1

Correspondence to:
J. M. Monteiro,
jmm@caos.iisc.ernet.in

Citation:
Monteiro, J. M., Á. F. Adames, J. M. Wallace, and J. S. Sukhatme (2014), Interpreting the upper level structure of the Madden-Julian oscillation, *Geophys. Res. Lett.*, *41*, doi:10.1002/2014GL062518.

Received 12 NOV 2014
Accepted 21 NOV 2014
Accepted article online 26 NOV 2014

Interpreting the upper level structure of the Madden-Julian oscillation

Joy M. Monteiro[1,2], Ángel F. Adames[3], John M. Wallace[3], and Jai S. Sukhatme[1,2]

[1]Centre for Atmospheric and Oceanic Sciences, Indian Institute of Science, Bangalore, India, [2]Divecha Centre for Climate Change, Indian Institute of Science, Bangalore, India, [3]Department of Atmospheric Sciences, University of Washington, Seattle, Washington, USA

Abstract The nonlinear response of a spherical shallow water model to an imposed heat source in the presence of realistic zonal mean zonal winds is investigated numerically. The solutions exhibit elongated, meridionally tilted ridges and troughs indicative of a poleward dispersion of wave activity. As the speed of the jets is increased, the equatorial Kelvin wave is unaffected but the global Rossby wave train coalesces to form a compact, amplified quadrupole structure that bears a striking resemblance to the observed upper level structure of the Madden-Julian oscillation. In the presence of strong subtropical westerly jets, the advection of planetary vorticity by the meridional flow and relative vorticity by the zonally averaged background flow conspire to create the distinctive quadrupole configuration of flanking Rossby waves.

1. Introduction

The Madden-Julian oscillation (MJO) exhibits a distinctive upper tropospheric, planetary scale flow configuration shaped like a quadrupole, which follows the region of anomalously strong or weak equatorial convection as it propagates eastward across the Indo-Pacific warm pool. The centers of the four gyres are located near 28°N/S, just equatorward of the climatological location of the subtropical jet streams, with cyclonic gyres to the east of the heat source and anticyclonic gyres to the west of it. This quadrupole pattern has been documented in studies of *Knutson and Weickmann* [1987], *Rui and Wang* [1990], and *Hendon and Salby* [1994], and is referred to in *Adames and Wallace* [2014] as the signature of "flanking Rossby waves".

In the lower troposphere, the observed structure of the MJO more closely resembles the well-known stationary wave response to an equatorial heat source described by *Matsuno* [1966] and *Gill* [1980] (hereafter referred to as the Matsuno-Gill response), with a Kelvin wave to the east of the heat source and equatorial Rossby waves to the west of it. Not only are the MJO-related upper and lower tropospheric anomalous flow patterns of opposing polarity, as in the "first baroclinic mode" [*Gill*, 1980]: the upper tropospheric pattern differs significantly from the canonical (i.e., linear, base state of rest on an equatorial β plane) Matsuno-Gill response, which is strongly localized within the equatorial belt. Using a two-layer shallow water model linearized about the observed upper level November-April winds, *Barlow* [2012] showed that the presence of subtropical westerlies in the background flow yields a forced, anticyclonic Rossby wave response to the west of the heating that extends into the subtropics. Motivated by the results of this numerical experiment, *Adames and Wallace* [2014] suggested that the upper tropospheric structure of the MJO is strongly influenced by the meridional and vertical shear of the climatological mean zonal flow: they argued that the jet streams serve as a waveguide for the flanking Rossby waves and as a barrier for the poleward dispersion of wave activity.

Here we investigate the role played by the zonal mean zonal winds in generating the distinctive upper tropospheric quadrupole flow configuration of the MJO. This objective is achieved by examining the stationary wave response to an equatorial heat source in a spherical nonlinear shallow water model with a zonal wind profile that approximates the observed upper atmospheric winds. The behavior of forced equatorial waves in the presence of mean zonal winds has been examined previously: see, for example, *Lau and Lim* [1982] and *Lim and Chang* [1983] for linear calculations on an equatorial β plane and *Lau and Lim* [1984] for linear and nonlinear calculations on the sphere. All the above numerical experiments yielded a Rossby wave train with a northwest-southeast tilt. More recently, *Kraucunas and Hartmann* [2007] used a meridionally varying bottom topography to prescribe a mean flow in their study of seasonal contrasts in the structure of the observed climatological mean stationary waves. *Bao and Hartmann* [2014] also used a

setup similar to *Kraucunas and Hartmann* [2007] to explore the effects of a zonally asymmetric jet on the Rossby wave response.

In the present work, rather than interpreting the shallow water system in terms of a modal decomposition of the full atmosphere, we model the upper atmosphere as a single layer and systematically investigate the effects of mean subtropical jets on the stationary response to equatorial heating. A striking feature noted is the transition from elongated, meridionally tilted Rossby waves to a compact, quadrupole structure that is localized just equatorward of the subtropical jet maximum. The vorticity balance implied by this transition is outlined, and its implications for the upper level structure of the MJO are discussed.

2. Experimental Setup

The model used in the experiments is the Geophysical Fluid Dynamics Laboratory Flexible Modeling System spherical nonlinear shallow water model (http://data1.gfdl.noaa.gov/~arl/pubrel/m/atm_dycores/doc/). Shallow water models have been used successfully to study stationary and quasi-stationary wave responses in both the extratropics [*Held*, 1983] and the tropics [*Kraucunas and Hartmann*, 2007; *Barlow*, 2012; *Bao and Hartmann*, 2014]. In our setup, the resting depth of the fluid is the same at all latitudes and a mean flow is generated by prescribing a meridionally varying bottom topography of the form $H_B = H_0[1 - (\sin\theta - \sin,\theta_0)^N]$, where H_0, N, and θ_0 are the maximum height, the power to which $\sin\theta$ is raised, and a reference latitude, respectively. The gradients of H_B act as forcing terms in the momentum equations in the model. In our case, only the v (meridional momentum) equation has a nonzero forcing term because H_B is zonally symmetric (Table S1 in the supporting information describes the mathematical model that we use). In all our experiments, $\theta_0 = 0$, implying an equatorially symmetric basic state. N controls the flatness of the gradient of H_B, and we set $N = 2$ following previous work [*Kraucunas and Hartmann*, 2007; *Bao and Hartmann*, 2014]. This choice also ensures the existence of westerly winds near the equator, which is necessary for the (equatorially trapped) Matsuno-Gill solution to have any influence outside the tropics [*Garcia and Salby*, 1987; *Sardeshmukh and Hoskins*, 1988]. In the β plane solutions $f = \beta y$, where β is set to its equatorial value $2\Omega/a$, Ω being the Earth's rotation rate and a the Earth's radius.

The location of the jets is controlled mainly by two parameters: N and the local Rossby radius of deformation $\sqrt{gH}/f$ where g, H, and f are acceleration due to gravity, the mean layer depth, and the vertical component of the planetary rotation, respectively. Physically, H_B represents the forcing of the flow toward the pole on isentropic surfaces due to the outflow from the rising branch of the Hadley circulation [*Pauluis et al.*, 2008]. Even though N and H are prescribed independently in our model, it must be noted that they are interdependent in the real atmosphere: they act in combination to control the location of the jets.

Experiments were conducted for a range of different values of H, but a value of 800 m was adopted for all experiments to ensure that the jets are located at around 30°N (Figure 1 of *Bao and Hartmann* [2014] shows the response for different values of H. See also Figure S1 in the supporting information). The winds and fluid depth are relaxed toward zero and the resting depth with time scales of $\kappa_M = 20$ and $\kappa_T = 10$ days, respectively. κ_T is chosen to represent the time scale of radiative cooling, and κ_M represents the time scale of vertical mixing from the lower layers and is kept small to ensure that the flow close to the equator approaches the angular-momentum-conserving limit [*Held and Phillips*, 1990]. The topographic forcing is linearly increased from zero to full H_B over a time span of 25 days to ensure a smooth spin-up of the model. The zonal mean zonal wind profiles shown in Figure 1 exhibit peaks at around 30°N/S with peak speeds ranging from 8 to 30 m/s. The observed wind speeds in the subtropical jets reach 30 m/s in the upper troposphere, and therefore, profile (d) corresponding to $H_0 = 2000$ m can be considered representative of the observed upper tropospheric conditions.

The system is forced with a Gaussian-shaped perturbation of the form

$$Q = Q_0 \exp\left((\theta - \theta_p)^2/L_y + (\lambda - \lambda_p)^2/L_x\right) - \overline{Q}(\theta) \tag{1}$$

$\overline{Q}(\theta)$, the zonal mean of the Gaussian, is subtracted out to prevent a zonal mean response from developing in the model. Subtracting $\overline{Q}(\theta)$ out has the effect of introducing a mass sink in the model in the same latitude belt as the Gaussian-shaped perturbation. For all experiments, the values of the various parameters in the above equation are $Q_0 = 100$ m, $\theta_p, \lambda_p = 0, 90$ degrees, and $L_x, L_y = 30, 10$ degrees. The spatial

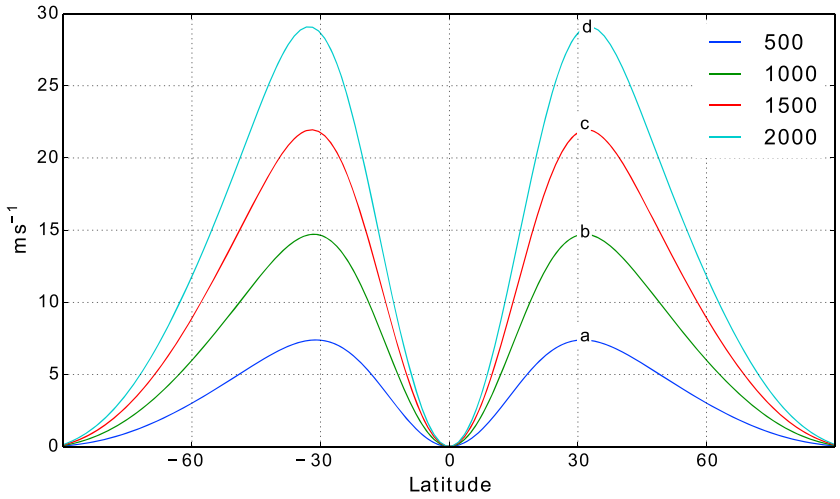

Figure 1. The zonal mean zonal wind for various values of H_0. The profiles are annotated with the letter corresponding to the panels in Figure 2.

scale was selected following *Barlow* [2012], and its amplitude is the same as that prescribed in *Kraucunas and Hartmann* [2007]. In all runs the model is spun up gradually over 25 days, and a nearly steady state is reached by day 45. Results are presented for day 99, unless otherwise noted.

3. Results

The response to an equatorial heat source, as expressed in the eddy geopotential and wind fields, are shown in Figure 2 for the various experiments. In Figures 2a and 2b the response of an atmosphere at rest on a β plane and for realistic spherical geometry is shown. These two panels form part of a family of solutions for varying values of the rotation of the planet presented in Figure S2 in the supporting information. In the solutions for low rotation rates, the β plane solutions extend to higher latitudes than those based on spherical geometry. Since the wave response is limited by the equatorial Rossby radius of deformation $\sqrt{c/\beta}$ ($c = \sqrt{gH}$), for Earth-like (or larger) rotation rates the wave response is confined to low latitudes where the β plane approximation holds good and the β plane solution closely approximates the full spherical solution.

When a weak zonal flow is prescribed, as is the case with $H_0 = 500$, the response assumes the form of a Rossby wave train with meridionally tilted ridges and troughs indicative of a poleward dispersion of wave activity as seen in Figure 2c. This wave train extends beyond the latitude at which the jet speed is maximum. The wave trains emanate from the perturbation at the equator centered at 90°E and reach their turning latitude around 60°N/S. A similar response was obtained by *Lau and Lim* [1984] for a zonal wind of 10 m/s with no meridional variation. The similarity of the solutions suggests that a weak westerly jet or superrotation with $U \leq 10$ m/s does not impede the poleward dispersion of the Rossby wave response.

As H_0 is increased, as shown in successive panels in Figure 2, the following features are noted:

1. The Rossby wave train widens meridionally, and the tilted troughs poleward of the heat source coalesce to form cyclonic gyres centered at 28°N/S, just equatorward of the jets (Figures 2c and 2d). With the further strengthening of the jets, the gyres shift eastward, until for a realistic jet strength, they are positioned about 40° of longitude to the east of the equatorial heat source (Figure 2f).
2. Following the formation of the cyclonic gyres, further increases in the prescribed zonal wind speed cause the tilted ridges to the west of the heat source to coalesce to form anticyclonic gyres, also centered along 28°N/S (Figure 2e). With the further strengthening of the jets, these gyres shift eastward and assume their positions as the western poles of the quadrupole configuration centered on the heat source (Figure 2f).
3. The geopotential height anomalies in the gyres are stronger, by roughly a factor of 5, than those in the tilted ridges and troughs in Figure 2c, and they are also much stronger than those in the equatorial

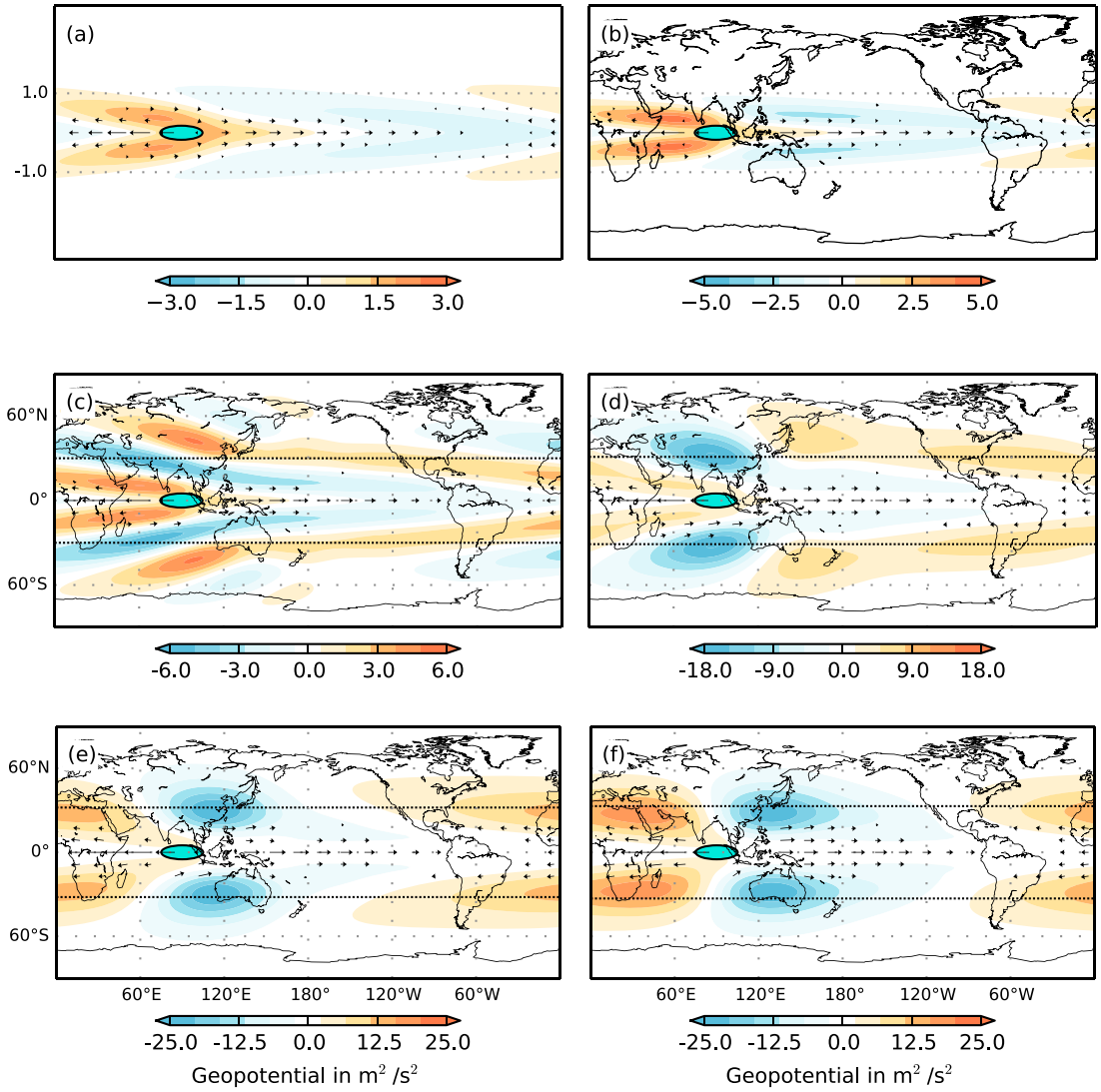

Figure 2. (a,b) Stationary eddy geopotential field and winds for the zero basic state flow simulations for a β plane and spherical geometry, respectively. The latitude lines correspond to an equatorial Rossby radius of deformation of ±1.0. (c–f) Stationary eddy geopotential and wind fields for H_0 = 500, 1000, 1500, and 2000 m, respectively. The location of the perturbation is marked by a turquoise ellipse in all panels. The longest arrow in all panels corresponds to a wind speed of around 0.7 m/s. In Figures 2c–2f, the location of the jet maxima is marked with latitude lines.

Kelvin waves. However, once they form, the gyres do not amplify substantially in response to a further strengthening of the jet streams.

4. The poleward energy dispersion is not as prominent in the quadrupole configuration (Figures 2e and 2f) as in the solution for the weak jets (Figure 2c), but it is still discernible. It appears that strong jets block the dispersion of wave activity toward higher latitudes.

A useful diagnostic for characterizing the linearity of the response to the amplitude of the heating is ρ_{MJO}, defined as the ratio of the maximum of the geopotential anomalies to the maximum of the zonal wind anomalies. It increases from a value of 8 in Figure 2c to 36 in Figure 2f. This is roughly comparable to the value calculated from regression maps derived from the ERA-Interim data, which is 53 (see Figure 5b). It is interesting to note that ρ_{MJO} is quite insensitive to the amplitude of the prescribed perturbation: As we increase Q_0 from 100 m to 1000 m, ρ_{MJO} decreases from 36 to 32. This is in contrast to its strong sensitivity to the basic state zonal flow: An increase in jet speeds from around 8 m/s to 30 m/s causes a fourfold increase in ρ_{MJO}. Thus, the results that we obtain are quite robust with respect to changes in the equatorial heating and further suggest that the observed configuration is essentially a linear response to the prescribed heating.

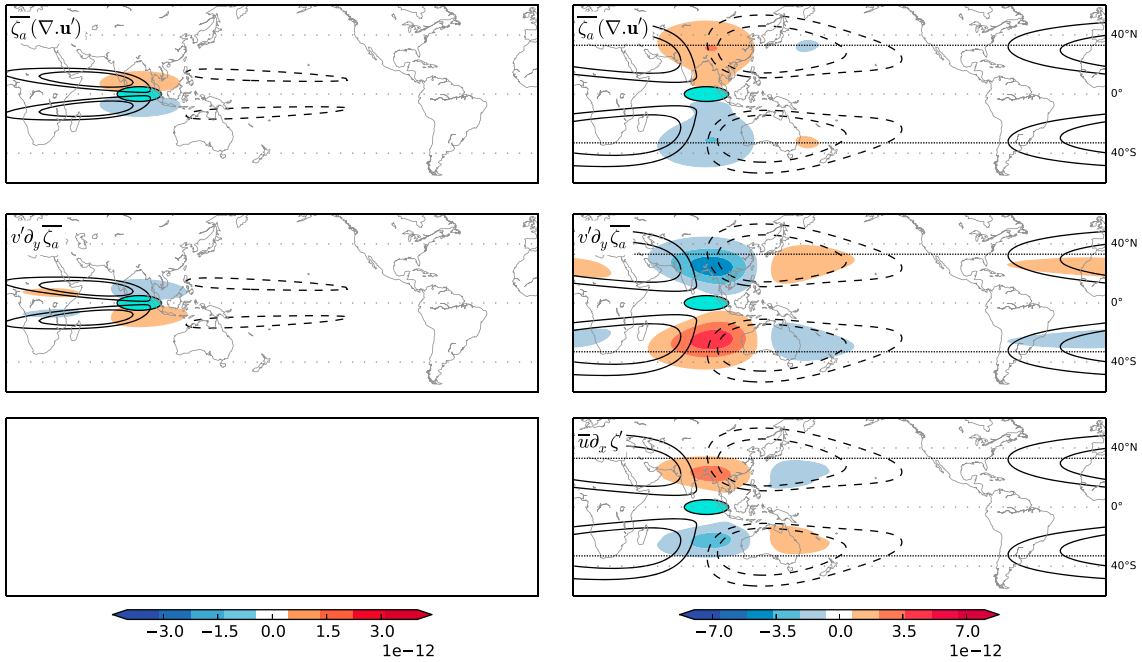

Figure 3. The vorticity balance in the (left) resting and (right) quadrupole simulations. The contour lines represent the geopotential contours corresponding to ±2, 3 (Figure 3, left) and ±5, 10 (Figure 3, right) m^2/s^2. $\overline{\zeta_a}$ denotes the planetary vorticity term $(f - \partial_y\overline{u})$.

3.1. Vorticity Balance

The vorticity balance for the stationary Rossby gyres can be best understood by considering the linear, steady state ($\partial_t\zeta = 0$), barotropic vorticity equation linearized about the mean zonal winds,

$$(f - \partial_y\overline{u})\nabla.\mathbf{u}' + v'\partial_y(f - \partial_y\overline{u}) + \overline{u}\partial_x\zeta' = 0. \quad (2)$$

where we partition a given field F into its zonal average and eddy fields, $F = \overline{F} + F'$. The zonal and meridional velocities are denoted by u and v, respectively. The relative vorticity is denoted by ζ.

The terms in equation (2) represent vorticity generation by the divergence, the meridional advection of planetary vorticity, and the advection of eddy relative vorticity by the zonal mean zonal winds, respectively. The corresponding fields for Figures 2b and 2f are shown in Figure 3. In the absence of mean winds, the equatorial balance (between ∼ 10°N/S) is between $v'\partial_y f$ and $f\nabla.\mathbf{u}'$, which is the equivalent of the Sverdrup balance in the atmosphere ($f\nabla.\mathbf{u}' = \beta v'$, see *Gill* [1980]). This is the balance that prevails in Figures 2a and 2b. With the inclusion of the subtropical jets the contribution of $\overline{u}\partial_x\zeta'$ increases nonlinearly in Figures 2c–2f due to the increase of $\overline{u}$, in combination with the amplification of the ζ' anomalies. The equatorial balance remains the same as in Figures 2a and 2b, while away from the equator $v'\partial_y(f - \partial_y\overline{u})$ is balanced by contributions from $\overline{u}\partial_x\zeta'$ and $(f - \partial_y\overline{u})\nabla.\mathbf{u}'$. As seen in Figure 3, equatorward of the jet maxima $\overline{u}\partial_x\zeta'$ plays an important role in balancing $v'\partial_y(f - \partial_y\overline{u})$. Areas of divergence are observed extending away from the equator toward the nodes of the geopotential anomalies in the Rossby wave quadrupole. This is because the divergence balances the advection of geopotential by the mean zonal winds in the steady state ($\Phi_B(\nabla.\mathbf{u}') = -\overline{u}\partial_x\Phi'$, refer to Table S1 in the supporting information). Thus, $(f - \partial_y\overline{u})\nabla.\mathbf{u}'$ also plays an important role, especially on the poleward flank of the jet where the absolute vorticity is large.

3.2. The Transient Response and Sensitivity to Drag

To study the development of the response of the system to the imposed equatorial heating, the model was spun-up for 25 days, and on day 25, the heating was switched on instantaneously. The resulting response for days 30, 35, 40, and 45 are shown in Figure 4. The westward half of the quadrupole appears immediately as a response to the applied heating. The eastward half appears around day 35 and assumes its steady state form around day 40. This lag suggests that the eastward half of the quadrupole is also part of the response to the remote heat source and not due to local effects.

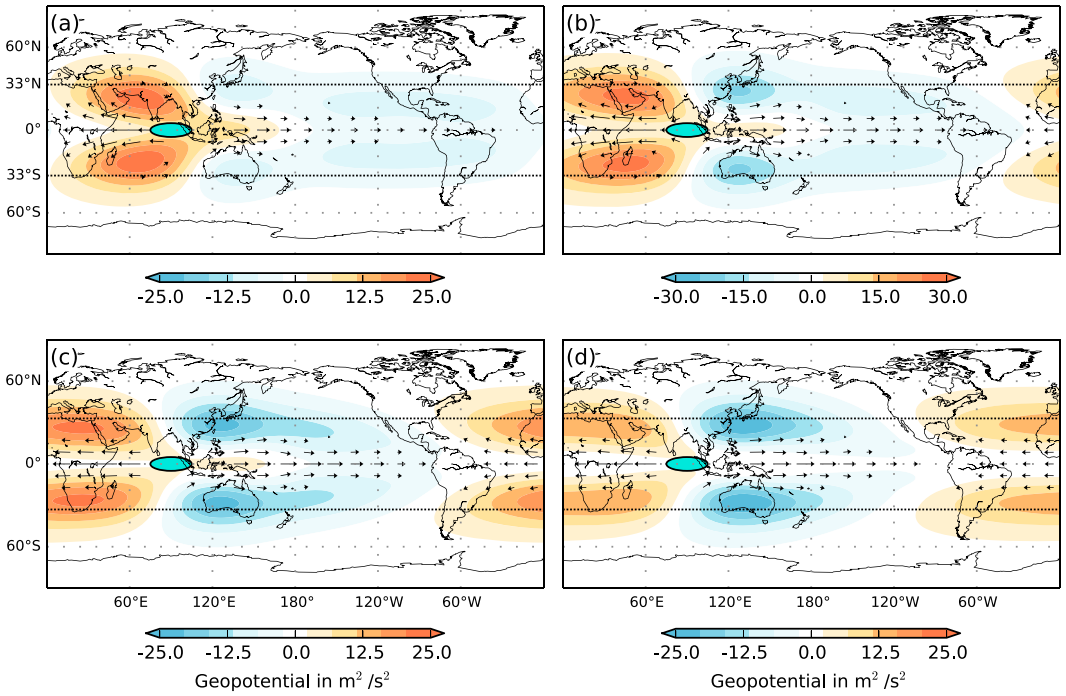

Figure 4. Transient solution showing the development of the quadrupole response. (a–d) The observed anomalies on days 30, 35, 40, and 45, respectively. The heat source is switched on day 25. The latitude lines mark the location of the jet maxima.

To determine the sensitivity of the results to the specified drag coefficient, the experiment in Figure 2f was repeated with relaxation time scales of $\kappa_M = \kappa_T = 1$, 5, 10, and 20 days (the results are presented in Figure S3 in the supporting information). In the high drag (short time scale) simulations, the waves are strongly damped as they disperse away from the equatorial heat source, consistent with the conclusions of *Gill* [1980]. As the drag is decreased, the quadrupole structure develops and the quadrupole pattern is well established when $\kappa_M = \kappa_T = 10$ days. Thus, the quadrupole structure seems to be insensitive to damping rates within the range of realistic values. The dominance of the western centers of the quadrupole in the

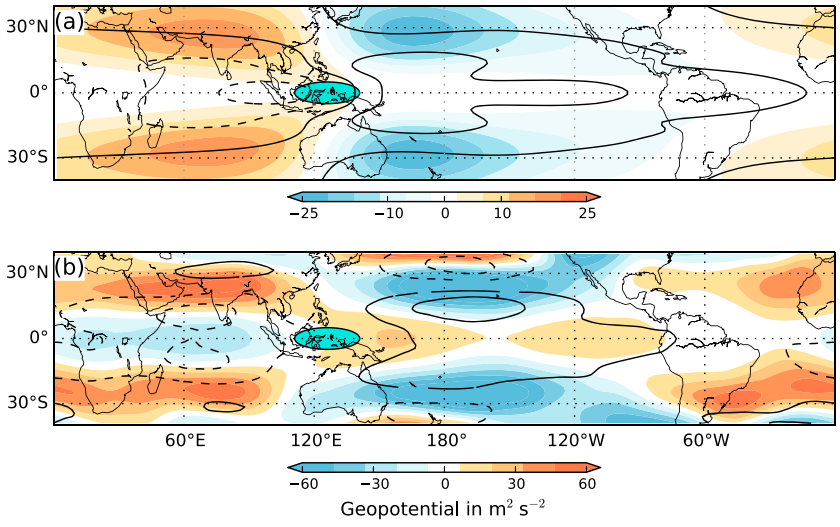

Figure 5. Comparison between the (a) simulated and (b) observed response to an equatorial heat source. The contours represent the eddy zonal wind component and the colored shading denotes the geopotential anomalies. Figure 5a depicts the same solution as in Figure 2f. Figure 5b is a reproduction of Figure 2c from *Adames and Wallace* [2014]. The contour interval in Figure 5a is 0.2 m/s and in Figure 5b is 0.6 m/s.

strongly damped, steady state solutions in Figures S3a and S3b of the supporting information is consistent with their more rapid setup in the transient solutions shown in Figure 4.

Finally, the observed patterns from *Adames and Wallace* [2014] and the simulated one are shown in Figure 5. The similarities are quite striking: The Rossby gyres in the quadrupole pattern are separated zonally by ~120° and are located around 28°N/S in both the observations and in the simulation. The location and sign of the zonal wind anomalies agree as well. The strength of the eastward half of the quadrupole (in terms of peak geopotential anomaly) is greater than that of the westward half in both observations and our simulated response. However, the equatorial geopotential response corresponding to the Kelvin wave is muted in comparison to the observed response. This is probably due to the presence of the mass sink which reduces the extent of the Kelvin wave by establishing mass/vorticity balance with greater efficiency than the monopole system in *Gill* [1980]. The simulated quadrupole structure is also slightly wider in meridional extent that the observed.

4. Discussion

In the preceding sections, we have presented the results of numerical experiments that shed light on the structure of tropical stationary waves. Specifically, we have shown how the presence of subtropical jets modify the well-known Matsuno-Gill response, with a Kelvin wave to the east of the heat source and Rossby waves to the west of it. The equatorial Kelvin wave is virtually unaffected by these modifications, but the Rossby waves are transformed into a quadrupole structure, trapped by the subtropical jets that bear a striking resemblance to the observed upper tropospheric (150 hPa) structure of the MJO, as represented in the observational study of *Adames and Wallace* [2014].

It is important to note that even though the equations that we use are similar to those used in the Matsuno-Gill model, the physical interpretation of the models is quite different: the Matsuno-Gill model represents the first baroclinic mode of the troposphere and is a linear model, whereas our model is a nonlinear representation of a layer in the upper troposphere, more in the spirit of *Held and Phillips* [1990].

We see that the response varies linearly with the amplitude of the heating and is a result of dry dynamics. The lag in the transient response and the emergence of the eastward half of the quadrupole only at low damping rates together suggest that the full quadrupole structure is a response to the heat source alone and not a linear combination of responses to the source and sink terms. The presence of a westerly meridional wind shear close to the equator is essential in enabling the equatorial response to break away from the equatorial waveguide and penetrate into the subtropics [*Lau and Lim*, 1984; *Garcia and Salby*, 1987; *Kraucunas and Hartmann*, 2007; *Barlow*, 2012]. In fact, if N in our experimental setup is increased from 2 to 8, which shifts the axes of the jets from 30°N/S to 60°N/S, the quadrupoles disappear and the equatorial response resembles the Matsuno-Gill response.

In the presence of strong subtropical westerly jets, the advection of planetary vorticity by the meridional flow and relative vorticity by the zonally averaged background flow conspire to create the MJO's distinctive quadrupole configuration of flanking Rossby waves.

Acknowledgments

The authors thank Dargan Frierson for constructive comments, which helped in making our results more general. We also thank the two anonymous reviewers whose comments improved the arguments and presentation of this work. J.M.M. is supported by a travel grant from the Divecha Centre for Climate Change. J.M.M. also acknowledges the University of Washington's Visiting International Student Internship and Training (UW-VISIT) program for helping to arrange his visit to UW. Á.F.A. is supported by the National Science Foundation's Graduate Research Fellowship Program (NSF-GRFP) grant DGE-0718124. J.M.W. is supported by the National Science Foundation under grant ATM 1122989. Requests for data used in this paper can be directed to Joy M. Monteiro (jmm@caos.iisc.ernet.in)

The Editor thanks two anonymous reviewers for their assistance in evaluating this paper.

References

Adames, Á. F., and J. M. Wallace (2014), Three-dimensional structure and evolution of the MJO and its relation to the mean flow, *J. Atmos. Sci.*, *71*(6), 2007–2026.

Bao, M., and D. L. Hartmann (2014), The response to MJO-like forcing in a nonlinear shallow-water model, *Geophys. Res. Let.*, *41*(4), 1322–1328.

Barlow, M. (2012), Africa and West Asia, in *Intraseasonal Variability in the Atmosphere-Ocean Climate System*, edited by W. K.-M. Lau and D. E. Waliser, pp. 477–495, Springer Praxis Books, Springer, Berlin, Heidelberg.

Garcia, R. R., and M. L. Salby (1987), Transient response to localized episodic heating in the tropics. Part II: Far-field behavior, *J. Atmos. Sci.*, *44*(2), 499–532, doi:10.1175/1520-0469(1987)044<0499:TRTLEH>2.0.CO;2.

Gill, A. E. (1980), Some simple solutions for heat-induced tropical circulation, *Q. J. R. Meteorol. Soc.*, *106*(449), 447–462, doi:10.1002/qj.49710644905.

Held, I. M. (1983), Stationary and quasi-stationary eddies in the extratropical troposphere: Theory, in *Large-Scale Dynamical Processes in the Atmosphere*, edited by B. J. Hoskins and R. P. Pearce, pp. 127–168, Academic Press, London.

Held, I. M., and P. J. Phillips (1990), A barotropic model of the interaction between the Hadley Cell and a Rossby Wave, *J. Atmos. Sci.*, *47*(7), 856–869, doi:10.1175/1520-0469(1990)047<0856:ABMOTI>2.0.CO;2.

Hendon, H. H., and M. L. Salby (1994), The life cycle of the Madden-Julian oscillation, *J. Atmos. Sci.*, *51*(15), 2225–2237, doi:10.1175/1520-0469(1994)051<2225:TLCOTM>2.0.CO;2.

Knutson, T. R., and K. M. Weickmann (1987), 30–60 day atmospheric oscillations: Composite life cycles of convection and circulation anomalies, *Mon. Weather Rev.*, *115*(7), 1407–1436.

Kraucunas, I., and D. L. Hartmann (2007), Tropical stationary waves in a nonlinear shallow-water model with realistic basic states, *J. Atmos. Sci.*, *64*(7), 2540–2557.

Lau, K.-M., and H. Lim (1982), Thermally driven motions in an equatorial β-plane: Hadley and Walker circulations during the winter monsoon, *Mon. Weather Rev.*, *110*(5), 336–353, doi:10.1175/1520-0493(1982)110<0336:TDMIAE>2.0.CO;2.

Lau, K.-M., and H. Lim (1984), On the dynamics of equatorial forcing of climate teleconnections, *J. Atmos. Sci.*, *41*(2), 161–176, doi:10.1175/1520-0469(1984)041<0161:OTDOEF>2.0.CO;2.

Lim, H., and C.-P. Chang (1983), Dynamics of teleconnections and Walker circulations forced by equatorial heating, *J. Atmos. Sci.*, *40*(8), 1897–1915, doi:10.1175/1520-0469(1983)040<1897:DOTAWC>2.0.CO;2.

Matsuno, T. (1966), Quasi-geostrophic motions in the equatorial area, *J. Meteor. Soc. Jpn.*, *44*(1), 25–43.

Pauluis, O., A. Czaja, and R. Korty (2008), The global atmospheric circulation on moist isentropes, *Science*, *321*(5892), 1075–1078.

Rui, H., and B. Wang (1990), Development characteristics and dynamic structure of tropical intraseasonal convection anomalies, *J. Atmos. Sci.*, *47*(3), 357–379.

Sardeshmukh, P. D., and B. J. Hoskins (1988), The generation of global rotational flow by steady idealized tropical divergence, *J. Atmos. Sci.*, *45*(7), 1228–1251, doi:10.1175/1520-0469(1988)045<1228:TGOGRF>2.0.CO;2.